

Efficient Semi-Supervised Federated Learning for Heterogeneous Participants

Zhipeng Sun, Yang Xu, *Member, IEEE*, Hongli Xu, *Member, IEEE*, Zhiyuan Wang, Yunming Liao
School of Computer Science and Technology, University of Science and Technology of China, Hefei, China
Suzhou Institute for Advanced Research, University of Science and Technology of China, Suzhou, China
{rodman, cswangzy, liaoyun}@mail.ustc.edu.cn, {xuyangcs, xuhongli}@ustc.edu.cn

Abstract—Federated Learning (FL) has emerged to allow multiple clients to collaboratively train machine learning models on their private data. However, training and deploying large-scale models on resource-constrained clients is challenging. Fortunately, Split Federated Learning (SFL) offers a feasible solution by alleviating the computation and/or communication burden on clients. However, existing SFL works often assume sufficient labeled data on clients, which is usually impractical. Besides, data non-IIDness across clients poses another challenge to ensure efficient model training. To our best knowledge, the above two issues have not been simultaneously addressed in SFL. Herein, we propose a novel Semi-SFL system, which incorporates clustering regularization to perform SFL under the more practical scenario with unlabeled and non-IID client data. Moreover, our theoretical and experimental investigations into model convergence reveal that the inconsistent training processes on labeled and unlabeled data have an influence on the effectiveness of clustering regularization. To this end, we develop a control algorithm for dynamically adjusting the global updating frequency, so as to mitigate the training inconsistency and improve training performance. Extensive experiments on benchmark models and datasets show that our system provides a $3.0\times$ speed-up in training time and reduces the communication cost by about 70.3% while reaching the target accuracy, and achieves up to 5.1% improvement in accuracy under non-IID scenarios compared to the state-of-the-art baselines.

Index Terms—Federated Learning, Split Learning, Semi-Supervised Learning, Clustering Regularization

I. INTRODUCTION

Recently, vast amounts of data generated by mobile and Internet of Things (IoT) devices have exhibited great potential for improving the performance of various applications. To process these data from both privacy and economic perspectives, Federated Learning (FL) [1] has emerged and been extensively applied in many AI applications, including intelligent medical [2], finance [3] and smart home [4]. In order to capture complex patterns and relationships in massive data, large-scale models have achieved better generalization and higher accuracy in various tasks [5]. However, hardware limitations of clients and network bandwidth constraints between clients and remote servers pose restrictions on typical FL. This motivates Split Federated Learning (SFL) [6]–[8], a promising solution for efficiently training large-scale models.

In SFL, a full model is divided into two submodels, *i.e.*, a top model (close to the output layer) and a bottom model (close to the input layer), at an intermediate layer (called *split layer*). The top model is updated on the server, while the

bottom model is trained on each client. During training, clients transmit activations (also called *features*) of the split layer to the server, which further performs forward and backward propagation on the top model with the features and returns the corresponding gradients. For example, given an 8-layer AlexNet with the size of 137 MB, when splitting the model at the 5th layer, the sizes of its bottom model and features are about 9 MB and 1 MB, respectively. Accordingly, model splitting contributes to reducing computation burden and communication costs for clients. Besides, since clients have access to only the bottom models, the privacy of the model’s complete structure is protected.

Despite the above benefits of SFL, two critical issues have to be addressed in SFL. Firstly, it is usually impractical that SFL always has access to fully labeled data for model training. Considering that data annotation is time-consuming and probably requires domain-specific expert knowledge, it is challenging to obtain sufficient labels, which makes large amounts of valuable unlabeled data untapped. Secondly, the clients usually belong to different individuals and/or work under different circumstances, thus data generated by different clients probably are non-Independent and Identically Distributed (non-IID). Models trained on non-IID data across different clients usually exhibit varying divergences [9], which will result in performance degradation.

To our best knowledge, the above two issues have not been addressed in SFL literature up to now. We are encouraged to find some inspiration in previous FL works. To make full use of unlabeled data, many FL works [10], [11] integrate the techniques of semi-supervised learning and propose Semi-supervised FL (termed Semi-FL). Some Semi-FL works assume clients possess labeled data while the server has unlabeled data [12], [13]. However, considering the lack of sufficient expert knowledge and/or labor, clients probably have more unlabeled data. Herein, we focus on a more practical scenario, where labeled data are maintained by the server and unlabeled data reside on the clients [14], [15]. In this case, Semi-FL first performs server-side supervised training on the labeled data, and then conducts client-side semi-supervised training on the unlabeled data using techniques like pseudo-labeling [16]–[19]. For example, Diao *et al.* [16] directly distribute and employ the up-to-date global model to generate pseudo-labels for the unlabeled data, and further train the local models (replicas of the global model) on clients in parallel.

As in typical FL, the non-IID issue inevitably reduces the generalization ability of trained models in [16].

For the non-IID issue in Semi-FL, many researchers have made efforts to improve the quality of pseudo-labels. For example, each client in [17] is provided with multiple helpers (*i.e.*, models of other clients with similar predictions given the same input) to generate high-quality pseudo-labels, but at the expense of increased communication costs. To limit the communication costs, an Exponential Moving Average (EMA) model (regarded as a *teacher* model) is constructed and widely utilized to guide the updating of each client’s local model (regarded as a *student* model) through pseudo-labeling [18], [19]. As the teacher models retain not only the generalized knowledge from historical teacher models but also the personalized knowledge from recent global models, they can help to promote the semi-supervised training on clients well. Besides the teacher models, some literature [20] employs a pre-trained model to initialize the global model and guide the aggregation of student models, so as to further improve the training performance. However, all the existing Semi-FL arts necessitate full models for semi-supervised learning on clients, which is not applicable in SFL, since clients possess only the bottom models.

To advance SFL in utilizing unlabeled data, it is intuitive to incorporate semi-supervised learning in SFL. In a naive Semi-supervised SFL (Semi-SFL) solution, both the global model and the teacher model are split and their bottom models are allocated to the clients. It mainly involves two alternate phases in a training round: i) server-side supervised training, where the server updates the global and teacher models with generally IID labeled data, and ii) cross-entity semi-supervised training, where client-side teacher/student bottom models produce the teacher/student features with non-IID data, which are separately sent and fed to the server-side top model for pseudo-labeling and model training. However, this solution only adopts the output logits and pseudo-labels for loss calculation, failing to adequately tackle the non-IID issue (refer to Section V).

To this end, we review the distinct properties of SFL and propose a novel Semi-SFL system that incorporates *Clustering Regularization* to perform SFL with unlabeled data. In Semi-SFL, the teacher bottom models inherit the advantages (*e.g.*, high generalization ability) of teacher models. Considering that the student bottom models are gradually trained on the non-IID client data as training progresses, they are more likely to overfit the client data compared to the teacher bottom models. Thus, the student features usually suffer from non-negligible *feature shift* [21] and reduced representative ability. Fortunately, the clustering of teacher features provides a comprehensive view of the feature distribution, which is robust to data skewness. As a result, the clustering results can be utilized to regularize the student bottom models, so as to improve their generalization ability, which motivates the design of clustering regularization. Furthermore, according to our theoretical and experimental analysis in Section IV-A, the global updating frequency (*i.e.*, the number of times when

performing server-side supervised training in a round) has a complicated influence on model convergence, and it is quite challenging to adaptively adjust the global updating frequency to achieve satisfied training performance.

Our main contributions are summarized as follows:

- We develop a novel Semi-SFL system incorporating clustering regularization, which to the best of our knowledge is the first solution to simultaneously address the issues of unlabeled and non-IID data in SFL.
- We theoretically and experimentally investigate the impact of global updating frequency on model convergence. Building on these findings, we dynamically and adaptively regulate the global updating frequency in response to expected changes in supervised loss to guarantee the effectiveness and efficiency of our proposed system.
- We conduct extensive experiments to evaluate the performance of our system. The experimental results show our system provides a $3.0\times$ speed-up in training time by reducing 70.3% of the communication cost while reaching the target accuracy. Besides, it achieves accuracy improvements up to 5.1% under different non-IID settings compared to the state-of-the-art baselines.

II. BACKGROUND AND MOTIVATION

In this section, we provide a description of semi-supervised SFL, followed by an exploration of the underlying motivation behind our system design. For ease of expression, we list some key notations in Table I.

A. Semi-supervised Split Federated Learning

Split Federated Learning (SFL) [7] is a combination of Federated Learning (FL) [1] and Split Learning (SL) [22]. FL is designed to train ML models on distributed edge devices with privacy-preserving, while SL aims at reducing the computation cost of participants with limited resources. Therefore, SFL inherits the advantages of both FL and SL.

Similar to FL, a Parameter Server (PS) and N clients collaboratively train an ML model (denoted as \mathbf{w}) in SFL. The model is split into two submodels as $\mathbf{w} = (\mathbf{w}_s, \mathbf{w}_c)$. The bottom model \mathbf{w}_c and the top model \mathbf{w}_s separately reside on clients and the PS. In general, the PS randomly selects a subset $V_h \in V$, consisting of $N_h = |V_h|$ ($N_h \leq N$) active clients at round h . The selected clients with bottom models are instructed to send features [7] and ground-truth labels y_i ($i \in [V_h]$) to the PS. The PS then calculates the gradients of features for each client in parallel and sends them to clients while accumulating the gradients $\Delta\mathbf{w}_s$ of the top model. Afterward, the clients perform backpropagation to update their bottom models. At the end of each round, the PS aggregates bottom models to obtain a global model for further training.

However, considering the lack of sufficient expert knowledge or labor on clients, it is usually practical that most or even all data on clients are unlabeled while the PS possesses some labeled data annotated by domain experts [16], [19]. Thus, it is appealing to develop Semi-supervised SFL (Semi-SFL), where the complete dataset \mathcal{D} consists of labeled dataset \mathcal{D}_l

TABLE I: Key notations.

Notation	Semantics
N_h	number of active clients in round h
V_h	set of active clients in round h
\mathcal{D}_s	labeled dataset on the PS
\mathcal{D}_u	unlabeled dataset across clients
\mathbf{w}_s	top model on the PS
$\mathbf{w}_{c,i}$	bottom model on client i
\mathbf{w}_p	projection head on the PS
$\tilde{\mathbf{w}}$	teacher model
\mathbf{w}^h	model at the beginning of round h
$\mathbf{w}^{h+\frac{1}{2}}$	model after supervised training in round h
$F(\mathbf{w})$	loss function of the entire model
e_i	student features by client i
\tilde{e}_i	teachers features by client i
$f_s(\cdot)$	loss function for supervised training
$f_u(\cdot)$	loss function for semi-supervised training
H	# of aggregation rounds
K_s	# of iterations for server-side supervised training, <i>i.e.</i> , the global updating frequency
K_u	# of iterations for cross-entity semi-supervised training, <i>i.e.</i> , the cross-entity updating frequency
η_h	learning rate in round h

and unlabeled dataset \mathcal{D}_u , and $\mathcal{D}_u \triangleq \mathcal{D}_{u,1} \cup \mathcal{D}_{u,2} \cup \dots \cup \mathcal{D}_{u,N}$ ($\mathcal{D}_{u,i}$ is the dataset of client i). The loss function over a labeled data sample (x, y) and the model parameter $\mathbf{w} \in \mathbb{R}^d$ with d dimensions is defined as $\ell_s(x, y, \mathbf{w})$. Thus, considering the supervised training on the labeled dataset \mathcal{D}_l , the loss function is $\mathbb{E}_{x \in \mathcal{D}_l} \ell_s(x, y, \mathbf{w})$.

To leverage the vast amounts of unlabeled data on clients, recent studies have achieved promising results by enforcing model predictions on augmented data that deviate significantly from the data distribution. The objective is to ensure the alignment between these predictions with their corresponding pseudo-labels [23]. In other words, for a given unlabeled data sample x , the model's prediction of its weakly-augmented version is represented as a vector $q = (q_1, \dots, q_M) \in [0, 1]^M$, where $\sum_{m=1}^M q_m = 1$, and M is the number of classes. The pseudo-label for x is then defined as $\hat{q} = \arg \max_m q_m$, and is retained only if $\max_m q_m$ falls above the pre-defined confidence threshold τ .

Let \mathcal{H} denote the cross-entropy loss function, which measures the discrepancy between the predicted and true labels. The unsupervised training loss with consistency regularization can be represented as:

$$\ell_u(x, \mathbf{w}) = \mathbb{1}(\max_m(q_m) > \tau) \mathcal{H}(x, \hat{q}, \mathbf{w}) \quad (1)$$

Then the total training objective is expressed as:

$$F(\mathbf{w}^*) \triangleq \min_{\mathbf{w} \in \mathbb{R}^d} [\mathbb{E}_{x \in \mathcal{D}_l} \ell_s(x, y, \mathbf{w}) + \mathbb{E}_{x \in \mathcal{D}_u} \ell_u(x, \mathbf{w})] \quad (2)$$

B. Motivation for System Design

In Semi-FL, the consistency regularization loss encounters a major hurdle when the unlabeled data is non-IID among clients, as local models tend to favor locally abundant categories while potentially disregarding minorities. Although each client might train an expert model, the model divergence among clients is exacerbated when the pre-defined confidence

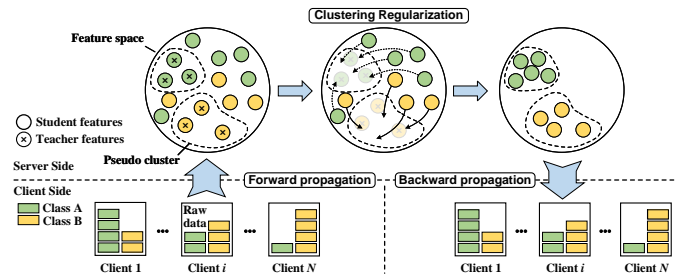


Fig. 1: Illustration of clustering regularization.

threshold (τ) blocks out data samples belonging to minority categories, especially in the early stages of training. Consequently, such imbalance in training leads to biased features [24], resulting in logits with low confidence which are more likely to be excluded from consistency regularization. Therefore, our objective is to effectively utilize the unlabeled data by exploring inter-client knowledge while ensuring efficient communication and computation.

Fortunately, the nature of SFL provides inspiration for a solution. In Semi-SFL, pseudo-labeling is performed on the PS where the top model resides. As shown in Fig. 1 (left), each client transmits two types of features for loss calculation: teacher features from the teacher bottom model (used for pseudo-labeling), and student features from the local bottom model (used for computing gradients). It is worth noting that the features collected on the PS show less skewness and higher abundance compared to those on each client. The fact that features are mutually accessible on the PS allows for leveraging the knowledge contained in features from multiple clients to mitigate the negative impact of non-IID data.

To this end, we propose to let the model learn more potential knowledge from features, enabling it to make confident predictions by identifying patterns and commonalities in the input. We modify a contrastive loss [25] for our purpose and propose *Clustering Regularization*. Concretely, for efficient processing, the features are first projected into lower-dimension vectors with the help of a two-layer linear network, *i.e.*, projection head. Subsequently, the (low-dimension) teacher features form different clusters (called *pseudo clusters*) regarding the pseudo-labels in the feature space, as illustrated in Fig. 1 (left). The contrastive loss then regularizes the projected student features of unlabeled samples to move towards the pseudo clusters of the same classes, as depicted in Fig. 1 (right). After clustering regularization, student features with the same pseudo-labels get closer to each other, which generates useful guideline information for model updating. Owing to the computation and communication-friendly framework of SFL, the execution of clustering regularization for all participating clients is completed on the PS, relieving clients from the corresponding computational and aggregation overhead.

Powered by clustering regularization, we can fully exploit the potential of unlabeled data, including the samples that are filtered by the confidence threshold and further excluded from consistency regularization. By leveraging the knowledge encoded in the pseudo clusters, even data samples belonging

to minority classes can contribute to model training. From another perspective, feature clustering assists and accelerates the process of consistency regularization, since well-clustered features provide data samples a higher chance to be credited with high confidence by the top model. Importantly, clustering regularization is not directly applied to the top model, which avoids introducing confirmation bias [25] and ensures that the model is always focused on the correct goal.

III. SYSTEM DESIGN

In our system, *cross-entity semi-supervised training* always follows the *server-side supervised training*. Such alternate training procedure will be conducted for H rounds. Fig. 2 illustrates the workflow of our system. In round h , our system workflow consists of the following five processes:

(1)-(2) **Supervised Training and Bottom Model Broadcast.** Initially, the PS trains a global model for K_s iterations using labeled data. The global model, denoted as $w = (w_c, w_s)$, consists of a bottom model w_c and a top model w_s . The model is originally designed to be trained with cross-entropy loss upon model outputs and ground-truth labels. Besides, a supervised-contrastive loss [26] is also employed as the loss function, which enables the model to learn similar or dissimilar representations with labels of the same or different classes. To facilitate the training process, an additional projection head w_h [27] is juxtaposed alongside w_s , receiving the output from w_c . Here, we define $g_w(\cdot)$ as the feed-forward function for model w . Let $\mathcal{B}_l \in \mathcal{D}_l$ represent any mini-batch from the labeled dataset. The loss function is defined as follows:

$$\mathcal{T}(x_j, w) = \frac{-1}{|P(j)|} \sum_{p \in P(j)} \log \frac{\exp(z_j \cdot z_p / \kappa)}{\sum_{a \in A(j)} \exp(z_j \cdot z_a / \kappa)} \quad (3)$$

where $z_j = g_{w_p}(g_{w_c}(x_j))$, $A(j)$ is the set of indexes in all reference samples except j , $P(j) \triangleq \{p \in A(j), y_p = y_j\}$ is the set of positive samples of image x_j , $\kappa \in \mathcal{R}^+$ is a scalar temperature parameter. In our formulation, the similar pairs consist of samples with the same label, while the dissimilar pairs consist of samples with different labels. The loss for supervised training is the summation over Eq. (3) and cross-entropy loss \mathcal{H} :

$$\ell_s = \mathcal{H} + \mathcal{T} \quad (4)$$

During training, an EMA model $\tilde{w} = (\tilde{w}_c, \tilde{w}_s, \tilde{w}_p)$ calculated as $\tilde{w} = \gamma \tilde{w} + (1 - \gamma)w$, $\gamma \in (0, 1]$ is employed as the teacher model. The teacher model shares the same model architecture as w , with its parameters being computed as a moving average of the global models trained in previous steps. It is utilized throughout the process to provide both pseudo labels and teacher features. To allow for loss calculation on abundant reference samples, we maintain a two-level memory queue \mathcal{Q} on the fly that caches the most recent features generated from the teacher model. The gradients of the supervised-contrastive loss only impose on the current mini-batch.

When global training is done in round h , a global model $w^{h+\frac{1}{2}} = w^{h, K_s}$ is obtained. Part of its components including the top model $w_s^{h+\frac{1}{2}}$, the projection head $w_p^{h+\frac{1}{2}}$ and their

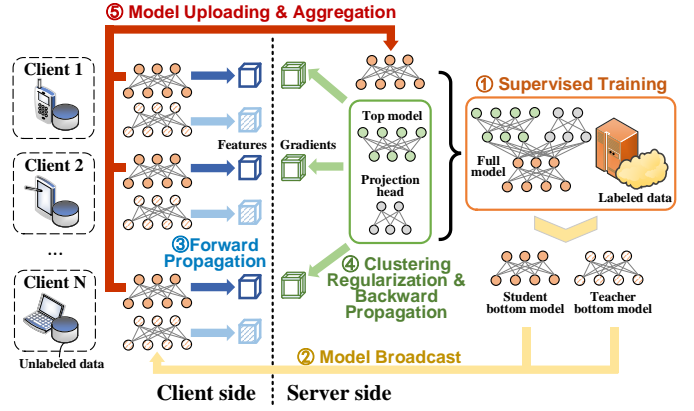


Fig. 2: System workflow.

teacher counterparts are kept on the server side, while the bottom model as $w_c^{h+\frac{1}{2}}$ and its teacher counterpart $\tilde{w}_c^{h+\frac{1}{2}}$ are broadcast to each client.

(3) **Forward Propagation.** Each cross-entity semi-supervised training round consists of K_u iterations, where K_u equals the cross-entity updating frequency. For client i , the bottom model in round h is initialized as $w_{c,i}^{h+\frac{1}{2},1} = w_c^{h+\frac{1}{2}}$. Before the k -th iteration, the bottom model and its teacher counterpart are notated as $w_{c,i}^{h+\frac{1}{2},k}$ and $\tilde{w}_{c,i}^{h+\frac{1}{2},k}$, respectively.

During the k -th iteration, client i performs cross-entity semi-supervised training on a batch size of $d_i^{h+\frac{1}{2},k}$. Considering the feed-forward process, any data sample x in a mini-batch $\mathcal{B}_{u,i} \subset \mathcal{D}_{u,i}$, $|\mathcal{B}_{u,i}| = d_i^{h+\frac{1}{2},k}$ first undergoes weak augmentation $a_w(\cdot)$, including random horizontal flipping and cropping, and strong augmentation $a_s(\cdot)$, exemplified by RandAugment [28] in our system. The productions are denoted as $a_w(x)$ and $a_s(x)$, respectively. They are then fed-forward to the bottom model $w_{c,i}^{k,t}$ and teacher bottom model $\tilde{w}_{c,i}^{k,t}$ in parallel, generating student features $e_i = (e_{i,1}, \dots, e_{i,|\mathcal{B}_{u,i}|})$ and teacher features $\tilde{e}_i = (\tilde{e}_{i,1}, \dots, \tilde{e}_{i,|\mathcal{B}_{u,i}|})$, where $e_{i,j} = g_{w_{c,i}^{h,k}}(a_s(x_{i,j}))$, $\tilde{e}_{i,j} = g_{\tilde{w}_{c,i}^{h,k}}(a_w(x_{i,j}))$, $x_{i,j} \in \mathcal{B}_{u,i}$. The student features e_i and teacher features \tilde{e}_i , each containing $d_i^{h+\frac{1}{2},k}$ samples, are then sent to the PS. On the PS, both the student and teacher features arriving at a synchronization barrier are then fed forward server-side models and their teacher counterparts in parallel.

(4) **Clustering Regularization & Backward Propagation.** As stated in section II-A, a cross-entropy loss is applied to minimize the prediction of noisy input, *i.e.*, a strongly-augmented sample and the pseudo-label. Additionally, to minimize the distance of model predictions of the same class in embedding space, we extend the contrastive loss to a multi-client setting. Based on notations of Eq. (3), we define the *Clustering Regularization* loss as:

$$\mathcal{C}(x_j, w) = \frac{-1}{|\hat{P}(j)|} \sum_{p \in \hat{P}(j)} \log \frac{\exp(z_j \cdot \tilde{z}_p / \kappa)}{\sum_{a \in [\mathcal{Q}]} \exp(z_j \cdot \tilde{z}_a / \kappa)} \quad (5)$$

where $z_j = g_{w_p}(e_j)$, $\tilde{z}_p = g_{\tilde{w}_p}(\tilde{e}_p)$ are projected student/teacher features, $\hat{P}(j) \triangleq \{p \in [\mathcal{Q}], \max_m(\tilde{q}_{p,m}) >$

$\tau, \tilde{q}_p = q_j\}$ is the set of the indexes of weakly-augmented samples that have the same pseudo-label with x_j and their confidences come up to τ . We follow the designation of contrastive regularization [25], while in our system the teacher model is instructed to guide the process. Specifically, the reference samples used for contrastive regularization are derived from the teacher features stored in the globally shared memory queue \mathcal{Q} , where features from prior supervised training are dequeued at a lower frequency. Our total loss over unlabeled data is composed of the consistency regularization term and clustering regularization term:

$$l_u = \mathcal{H} + \mathcal{C} \quad (6)$$

By performing backward propagation, the estimated gradients for client i computed as $\tilde{\nabla}_s f_{u,i}(\mathbf{w}_s^{h+\frac{1}{2},k}) = \frac{1}{|\mathcal{B}_{u,i}|} \sum_{x_{i,j} \in \mathcal{B}_{u,i}} \nabla l_{ce}(x_{i,j}, \mathbf{w}_s^{h+\frac{1}{2},k})$ and $\tilde{\nabla}_p f_{u,i}(\mathbf{w}_p^{h+\frac{1}{2},k}) = \frac{1}{|\mathcal{B}_{u,i}|} \sum_{x_{i,j} \in \mathcal{B}_{u,i}} \nabla l_c(x_{i,j}, \mathbf{w}_p^{h+\frac{1}{2},k})$ is kept until getting through all student features received before. Subsequently, the PS updates its server-side models with learning rate η_h as:

$$\begin{aligned} \mathbf{w}_s^{h+\frac{1}{2},k+1} &= \mathbf{w}_s^{h+\frac{1}{2},k} - \eta_h \frac{1}{N} \sum_{i \in [N]} \tilde{\nabla}_s f_{u,i}(\mathbf{w}_s^{h+\frac{1}{2},k}) \\ \mathbf{w}_p^{h+\frac{1}{2},k+1} &= \mathbf{w}_p^{h+\frac{1}{2},k} - \eta_h \frac{1}{N} \sum_{i \in [N]} \tilde{\nabla}_p f_{u,i}(\mathbf{w}_p^{h+\frac{1}{2},k}) \end{aligned} \quad (7)$$

Along with that, the gradients of student features e_i computed as $de_i = \{\nabla l_u(e_{i,j} \in [\mathcal{B}_{u,i}], \mathbf{w}_{c,i}^{h+\frac{1}{2},k})\}$ with a batch size of $d_i^{h+\frac{1}{2},k}$ are sent to the corresponding client i . Then each client continues to perform backward propagation $\tilde{\nabla}_c f_{u,i}(\mathbf{w}_{c,i}^{h+\frac{1}{2},k}) = \frac{1}{|\mathcal{B}_{u,i}|} \sum_{j \in [\mathcal{B}_{u,i}]} \nabla l_u(e_{i,j}, \mathbf{w}_{c,i}^{h+\frac{1}{2},k})$ and updates its student/teacher bottom model respectively, which is expressed as:

$$\begin{aligned} \mathbf{w}_{c,i}^{h+\frac{1}{2},k+1} &= \mathbf{w}_{c,i}^{h+\frac{1}{2},k} - \eta_h \tilde{\nabla}_c f_{u,i}(\mathbf{w}_{c,i}^{h+\frac{1}{2},k}) \\ \tilde{\mathbf{w}}_{c,i}^{h+\frac{1}{2},k+1} &= \gamma \tilde{\mathbf{w}}_{c,i}^{h+\frac{1}{2},k} + (1-\gamma) \mathbf{w}_{c,i}^{h+\frac{1}{2},k+1} \end{aligned} \quad (8)$$

(5) **Bottom Model Aggregation.** After total K_u iterations, clients upload their bottom models to the PS at a synchronization barrier, while the teacher bottom models, which are obtained from supervised training, are excluded from model uploading. The server-side models are set as $\mathbf{w}_s^{h+1} = \mathbf{w}_s^{h+\frac{1}{2},K_u+1}$ and $\mathbf{w}_p^{h+1} = \mathbf{w}_p^{h+\frac{1}{2},K_u+1}$. The PS aggregates the bottom models uploaded by clients to obtain a global bottom model $\mathbf{w}_c^{h+1} = \frac{1}{N} \sum_{i \in [V]} \mathbf{w}_{c,i}^{h+\frac{1}{2},K_u+1}$, which, together with the modules residing at the PS, is assembled for further supervised training.

IV. ALGORITHM DESIGN

In this section, we propose a greedy algorithm for global updating frequency adaptation, which is an important component of our system. We first analyze the convergence bound after H rounds *w.r.t.* both the global updating frequency and the cross-entity updating frequency. Then we will introduce our algorithm design and explain how it contributes to model convergence.

A. Convergence Analysis

Since the training is performed in an alternate manner, the convergence of the loss function relates to the training status in both the supervised training and cross-entity semi-supervised training stages. For the sake of analysis, we make the following assumptions as suggested in [29]–[32]:

Assumption 1. (Lipschitz Continuous Gradient) The loss function $F(\cdot)$ and loss components $f_s(\cdot)$ and $f_{u,i}(\cdot)$ of the entire model are L -smooth such that:

$$\begin{aligned} \|\nabla F(\mathbf{x}) - \nabla F(\mathbf{y})\| &\leq L \|\mathbf{x} - \mathbf{y}\|, \forall \mathbf{x}, \forall \mathbf{y} \\ \|\nabla f_s(\mathbf{x}) - \nabla f_s(\mathbf{y})\| &\leq L \|\mathbf{x} - \mathbf{y}\|, \forall \mathbf{x}, \forall \mathbf{y} \\ \|\nabla f_{u,i}(\mathbf{x}) - \nabla f_{u,i}(\mathbf{y})\| &\leq L \|\mathbf{x} - \mathbf{y}\|, \forall \mathbf{x}, \forall \mathbf{y} \end{aligned}$$

Assumption 2. (Bounded Second Moments) There exist constants G_s and G_u , such that the second moments of the stochastic gradients of the unsupervised loss and supervised loss on any data sample are upper bounded by:

$$\begin{aligned} \|\nabla l_u(x, \mathbf{w})\|^2 &\leq G_u^2, \forall x, \forall \mathbf{w} \\ \|\nabla l_s(x, \mathbf{w})\|^2 &\leq G_s^2, \forall x, \forall \mathbf{w} \end{aligned}$$

Assumption 3. (Unbiased Gradient Estimator) Let $\nabla f_s(\mathbf{w})$ denote the gradients derived from the labeled data on the PS and $\nabla f_{u,i}(\mathbf{w}_i)$ denote the gradients derived from the unlabeled data of client i , the gradient estimators are unbiased as:

$$\begin{aligned} \mathbb{E} \|\tilde{\nabla} f_s(\mathbf{w})\| &= \mathbb{E} \|\nabla f_s(\mathbf{w})\|, \forall \mathbf{w} \\ \mathbb{E} \|\tilde{\nabla} f_{u,i}(\mathbf{w})\| &= \mathbb{E} \|\nabla f_{u,i}(\mathbf{w})\|, \forall \mathbf{w} \end{aligned}$$

Based on those assumptions, we have the following results given an initialized model \mathbf{w}^0 (complete proof is presented in the Appendix):

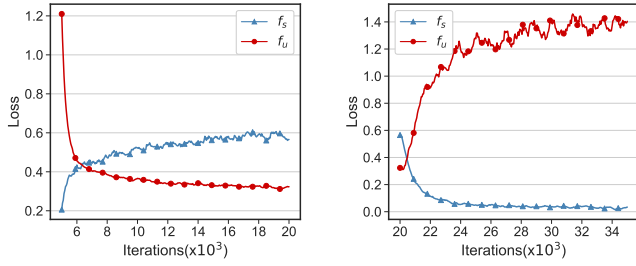
Theorem 1. The sequence of outputs $\{\mathbf{w}^{h,k}\}$ generated by supervised training and global aggregation satisfies:

$$\min_{h \in [H], k \in [K_s+1]} \mathbb{E} \|\nabla F(\mathbf{w}^{h,k})\|^2 \leq \frac{2(F(\mathbf{w}^0) - F(\mathbf{w}^*))}{\eta H K_s} + \Phi$$

where $\Phi \triangleq \left(\frac{L^2(K_u-1)(2K_u-1)\eta^2}{3K_s} + \frac{LK_u^2\eta^3}{K_s} + 1 \right) G_u^2 + (L\eta + \frac{2K_u}{K_s}) G_s^2$.

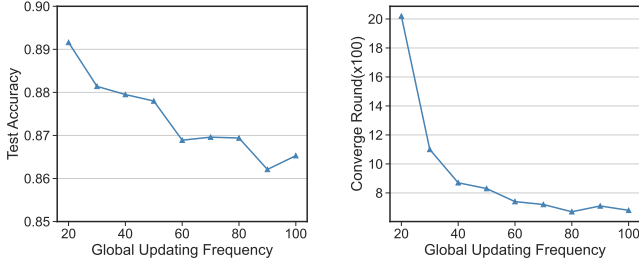
Theorem 1 suggests that the convergence of model training in an alternating manner is dependent on G_s^2 and G_u^2 . In fact, when η approaches 0, consecutive training on either supervised training or cross-entity semi-supervised training stage will lead to either G_s^2 or G_u^2 approaches 0. It implies that convergence can be ensured when the updating frequency on the other stage approaches 0. However, due to the alternate training, G_s^2 and G_u^2 might affect each other, resulting in fluctuations in Φ that hinder the convergence.

To provide evidence for this, an experiment is conducted on AlexNet, which is pre-trained on 4,000 labeled data samples from the CIFAR-10 dataset for 5,000 iterations. Initially, the model is trained over the unlabeled dataset using the pseudo



(a) Training on unlabeled data (b) Training on labeled data

Fig. 3: Loss variation on alternate training phases.



(a) Accuracy vs. K_s . (b) Round vs. K_s .

Fig. 4: Model training with different K_s .

labels predicted by the teacher model for 20,000 iterations. Then, the training is resumed over the labeled dataset for another 20,000 iterations. The variations of both f_s and f_u are recorded in Fig. 3. The results demonstrate that minimizing one of the losses (f_s or f_u) has negative effects on the other. The convergence can only be achieved if the positive effect always outweighs the negative effect. More generally, an equilibrium will be attained after sufficient training rounds if the effects of the two stages cancel each other out, and both the global updating frequency K_s and the cross-entity updating frequency K_u are the key factors that influence the equilibrium.

Next, we delve into a more detailed analysis based on the experimental observations. From Theorem 1, determining an optimal K_u to minimize the expected gradients is non-trivial. To simplify the problem, considering a fixed K_u , a larger global updating frequency is preferred to reach equilibrium faster (the expected gradients move faster towards G_u^2). However, as observed in Fig. 3, cross-entity semi-supervised training has a smaller impact on the supervised loss compared to vice versa. Consequently, a lower global updating frequency might contribute more to convergence (G_u^2 closer to 0). To observe the impact of global updating frequency, we conduct experiments by training AlexNets on the CIFAR-10 dataset using our proposed system with 10 clients. We set $K_u = 50$ and vary K_s . We record the aggregation rounds and test accuracy until the loss averaged over the last 10 rounds is reduced to less than a certain scalar (0.01), indicating reaching equilibrium. Fig. 4 shows that the model trained with a relatively smaller global updating frequency yields higher

model accuracy, at the expense of more aggregation rounds, *i.e.*, more resource consumption. As such, we face a dilemma in determining the global updating frequency.

B. Global Updating Frequency Adaptation

In the previous section, it is highlighted that obtaining a constant optimal global updating frequency in advance during training rounds is not feasible. To address this challenge, we present an algorithm for global updating frequency adaptation. Specifically, in each round, we estimate the supervised loss ℓ_s^{h+1} for the next round with a moving average. The PS then calculates the difference between two 10-round estimated loss averages as $\Delta\ell_s$. We enable the system to adjust the global updating frequency on several training milestones \mathcal{M} as:

$$K_s^{h+1} = \begin{cases} \frac{K_s^h}{2} & \text{if } |\Delta\ell_s^h| < \varrho_1 \text{ and } h \in \mathcal{M} \\ 2K_s^h & \text{if } |\Delta\ell_s^h| > \varrho_2 \text{ and } h \in \mathcal{M} \\ K_s^h & \text{otherwise} \end{cases} \quad (9)$$

where $0 < \varrho_1 < \varrho_2$ are priors.

Next, we will delve into our algorithm design. Initially, the model parameters are randomly initialized. At this stage, the model barely generates confident pseudo labels and mainly focuses on supervised training, resulting in a rapid reduction of the loss, *i.e.*, a high value of $|\Delta\ell_s^h|$. Since the few pseudo labels at the beginning may be biased, the model requires more attention on supervised training to update towards the correct goal. Therefore, we assign our system a larger global updating frequency to prioritize supervised training. As training progresses and the loss over the labeled data stabilizes, it signifies that sufficient attention has been given to the labeled data. Consequently, we instruct a lower global updating frequency to avoid hindering the cross-entity semi-supervised training stage. This ensures that the positive effects consistently outweigh the negative effects during the alternate training phases, enabling the model to achieve optimal performance. Moreover, our approach prevents over-reduction of the global updating frequency, which could otherwise increase confirmation bias [33], by using the high value of $|\Delta\ell_s^h|$ as a signal to adjust the global updating frequency. The results presented in the subsequent sections will demonstrate the significance of our adaptation algorithm.

We present the overall training process on the PS, including the adaptation algorithm, in Alg. 1. The training starts with supervised training, and the teacher model is updated batch-wise at the PS in each round for K_s^h iterations (Lines 4-5 in Alg. 1). The PS distributes the global bottom model and teacher bottom model to each client (Line 7 in Alg. 1). The cross-entity semi-supervised training on PS is performed for each client in turn using the top model. Then, the calculated gradients for student features are sent to the corresponding clients (Lines 10-13 in Alg. 1). After K_u steps of cross-entity semi-supervised training, the bottom models are aggregated (Lines 19-22 in Alg. 1). Finally, the PS updates K_s based on estimating the loss variation at the end of each round (Lines 23-24 in Alg. 1) and starts the next round. The client training

Algorithm 1 Training process on the PS

```
1: Initialize global model  $\mathbf{w} = (\mathbf{w}_c, \mathbf{w}_s, \mathbf{w}_p)$ , average
   model,  $\tilde{\mathbf{w}} = \mathbf{w}$ ,  $K_s^1 = K_s$ 
2: for  $h = 1$  to  $H$  do
3:   for  $k = 1$  to  $K_s^h$  do
4:     Update  $\mathbf{w}^{h,k+1} = \mathbf{w}^{h,k} - \eta_h \tilde{\nabla} f_s(\mathbf{w}^{h,k})$ 
5:     Update  $\tilde{\mathbf{w}}^{h,k+1} = \gamma \tilde{\mathbf{w}}^{h,k} + (1 - \gamma) \mathbf{w}^{h,k+1}$ 
6:   end for
7:   Send  $\mathbf{w}_c^{h+\frac{1}{2}}$  and  $\tilde{\mathbf{w}}_c^{h+\frac{1}{2}}$  to all workers and set  $\mathbf{w}_s^{h+\frac{1}{2},1} =$ 
    $\mathbf{w}_s^{h+\frac{1}{2}}$ ,  $\mathbf{w}_p^{h+\frac{1}{2},1} = \mathbf{w}_p^{h+\frac{1}{2}}$ 
8:   for  $k = 1$  to  $K_u$  do
9:     for  $i$  in  $V$  do
10:      Get  $(e_i, \tilde{e}_i)$  from client  $i$ 
11:      Forward propagation with  $e_i$  and  $\tilde{e}_i$  on  $(\mathbf{w}_s^{h+\frac{1}{2},k},$ 
    $\mathbf{w}_p^{h,k})$  and  $(\tilde{\mathbf{w}}_s^{h+\frac{1}{2},k}, \tilde{\mathbf{w}}_p^{h+\frac{1}{2},k})$ 
12:      Backward propagation, calculate  $\tilde{\nabla}_s f_{u,i}(\mathbf{w}_s^{h+\frac{1}{2},k})$ 
   and  $\tilde{\nabla}_p f_{u,i}(\mathbf{w}_p^{h+\frac{1}{2},k})$ 
13:      Send the gradients of  $e_i$  to client  $i$ 
14:     end for
15:     Update top models as Eq. (7)
16:   end for
17:   for  $i$  in  $V$  do
18:     Get  $\mathbf{w}_{c,i}^{h+\frac{1}{2},K_u+1}$  from client  $i$ 
19:   end for
20:   Set  $\mathbf{w}_c^{h+1} = \frac{1}{N} \sum_{i \in [N]} \mathbf{w}_{c,i}^{h+\frac{1}{2},K_u+1}$ 
21:   Estimate  $\ell_s^{h+1}$  and Update  $\Delta \ell_s^h$ 
22:   Update  $K_s^{h+1}$  as Eq. (9)
23: end for
```

process is identical to what we have described in Section III, which includes conducting local forward propagation, uploading features, and backward propagation based on the downloaded gradients subsequently.

V. EXPERIMENTS AND EVALUATION

In this section, we begin by providing a list of the datasets and models, as well as a description of the devices utilized in the experiments. We then introduce the adopted baselines and metrics for performance comparison. Finally, we present our evaluation results and analyze the superiority of our proposed system under various scenarios.

A. Datasets and Models

Datasets: We conduct experiments on three commonly used real-world datasets for semi-supervised learning: SVHN [34], CIFAR-10 [35], and IMAGE-100. The SVHN dataset contains 73,257 digits for training and 26,032 digits for testing, which are labeled in 10 classes. As suggested in [16], 1,000 labeled digits in the training set are allocated for the PS, while the remaining training data are distributed to clients as unlabeled data. The CIFAR-10 dataset is an image dataset consisting of 60,000 32×32 color images (50,000 for training and 10,000 for testing) in 10 categories, and 4,000 images are set as labeled data on the PS. To evaluate our proposed system on

a more challenging task, we create the IMAGE-100 dataset, which is a subset of ImageNet [36] and contains 100 out of 1,000 categories. Each sample in IMAGE-100 is resized to the shape of $144 \times 144 \times 3$, and 5,000 labeled images are allocated for the PS.

Models: Three models with different types and structures are adopted on the above three real-world datasets for performance evaluation: (i) CNN on SVHN, (ii) AlexNet [37] on CIFAR-10, (iii) VGG16 [38] on IMAGE-100. For SVHN, we train a customized CNN model with size of 3.35MB, which has two 5×5 convolutional layers, a fully-connected layer with 512 units, and a softmax output layer with 10 units. Besides, for CIFAR-10, we train the AlexNet model composed of three 3×3 convolutional layers, one 7×7 convolutional layer, one 11×11 convolutional layer, two fully-connected hidden layers, and one softmax output layer. Finally, the VGG16 model, which consists of 13 convolutional layers with kernel size of 3×3 , two fully-connected layers and a softmax output layer, is trained for image classification of IMAGE-100.

B. Baselines and Metrics

Baselines: We compare our proposed system with the following four baselines.

- **Supervised-only:** Supervised-only refers to using only the labeled dataset available on the PS for supervised training. This represents the lower bound that can be achieved with a limited amount of labeled data.
- **SemiFL** [16]: SemiFL is the first approach for semi-supervised FL with accuracy on par with standalone training. In SemiFL, pseudo-labels for the local data of each client are generated upon the latest global model. While in a certain iteration, each client applies the Mixup [39] technique on each data batch to augment the data and then perform forward and backward propagation using a specialized “mix” loss.
- **FedMatch** [17]: FedMatch learns inter-client consistency by mutual sharing of client models. To mitigate interference between supervised and semi-supervised tasks, FedMatch decomposes model parameters into two variables, which are updated in an alternate way.
- **FedSwitch** [19]: FedSwitch is the state-of-the-art approach that leverages an EMA model, *i.e.*, a teacher model, to ensure the quality of pseudo-labels. Additionally, it adaptively switches between the teacher and student model for pseudo-labeling, both to enhance the quality of pseudo-labels in non-IID settings and reduce communication costs.
- **FedSwitch-SL:** An extension version of FedSwitch that incorporates the technique of Split Learning (SL). It serves as an ablation study to demonstrate the effectiveness of our clustering regularization.

Metrics: We employ the following metrics to evaluate the performance of different systems.

- **Test accuracy:** In each round, we measure the accuracy of the global model on the test set with different baselines.

For FedSwitch(-SL) and our system, we use the global teacher model for testing.

- **Time cost:** We record the total time taken to achieve target test accuracy on different systems, which includes the time for computation and communication.
- **Communication cost:** The communication cost for transmitting models and feature batches (if any) to between entities achieve the target accuracy is also recorded.

C. Experimental Setup

We evaluate the performance of our proposed system on an AMAX deep learning workstation equipped with an Intel(R) Xeon(R) Gold 5218R CPU, 8 NVIDIA GeForce RTX 3090 GPUs, and 256 GB RAM. We simulate one PS and 30 clients on this workstation. To reflect the heterogeneity in the computation capabilities of clients, we assume that the computing time of one local iteration on each simulated client follows a Gaussian distribution. The mean and variance of the Gaussian distribution are derived from time records of performing one local iteration on various commercial edge devices, such as NVIDIA Jetson NX and AGX. Additionally, for simulating the network dynamics of wireless links between clients and the PS, the outbound bandwidths are implemented to fluctuate between 2Mbps and 8Mbps, and the inbound bandwidths vary between 10Mbps and 20Mbps, as suggested in [40]. We use the PyTorch deep learning framework for our software implementation of model training and build up the connections between clients and the PS using the socket library. The source code is available at <https://github.com/littlefisher/Capsule>.

We run 10 trials for all benchmark models and datasets with different random seeds. The standard errors are presented in the tables and the figures. By default, each experiment is run for 1,000 aggregation rounds on SVHN, CIFAR-10, and IMAGE-100 to ensure convergence. During each round, $N_h = 10$ clients are randomly selected to participate in the training process. Similar to [16], we use an SGD optimizer to optimize the models and adopt the cosine learning rate decay schedule [41]. Besides, we set the same hyperparameters as in [16], where the optimizer momentum $\beta_l = 0.9$, the initial learning rate $\eta = 0.02$, and the confidence threshold $\tau = 0.95$. As for the adaptation algorithm, we set $\varrho_1 = 0.01$ and $\varrho_2 = 0.05$. Unless otherwise specified, the number of labeled data samples on the PS is 1,000, 4,000, and 20,000 for SVHN, CIFAR-10, and IMAGE-100, respectively, and the unlabeled data samples are distributed uniformly across clients.

D. Experiment Results

1) *Overall Effectiveness:* The final test accuracies on SVHN, CIFAR-10, and IMAGE-100 for our system and baselines are presented in Table II. Supervised-only is omitted in the later sections for the comparison of training efficiency since the clients are not involved in this approach.

In terms of accuracy, our proposed system consistently achieves the highest accuracy compared to state-of-the-art approaches. For instance, on the SVHN dataset, our system achieves 91.4% accuracy, which is 2.3% higher than that in

TABLE II: Overall test accuracy (%).

Baseline	Dataset		
	SVHN	CIFAR-10	IMAGE-100
Supervised-only	73.6(0.24)	75.1(0.52)	26.1(0.73)
SemiFL	88.1(0.72)	86.8(1.23)	65.4(2.02)
FedMatch	88.4(0.56)	86.1(1.06)	29.6(1.70)
FedSwitch	89.0(0.46)	87.9(1.04)	60.3(1.51)
FedSwitch-SL	89.1(0.36)	87.5(0.79)	61.1(1.43)
Ours	91.4(0.49)	88.7(1.13)	66.5(1.79)

FedSwitch-SL. Similarly, our system achieves 88.7% accuracy on CIFAR-10, surpassing SemiFL by 1.2%. Moreover, on IMAGE-100, our system achieves 61.1% accuracy, which exhibits a 5.4% improvement over FedSwitch-SL. Our system also improves accuracy from 2.6% to 36.9% compared to FedMatch across the three datasets, highlighting the effectiveness of our proposed clustering regularization.

Moreover, the results indicate a naive integration of SemiFL techniques, such as combining FedSwitch with Split Learning, does not yield substantial improvements in overall accuracy. Additionally, FedMatch, which is specifically crafted to address the non-IID issue within the context of CIFAR-10, fall short in achieving superior performance on more complicated tasks, like the IMAGE-100 classification. That can be attributed to its model parameter decomposition strategy, which leads to ineffective batch normalization over separate hidden input features. It is worth noting that the accuracy gap between our model and the model trained only with labeled data is over 40% on IMAGE-100. This result strongly indicates the importance and necessity of our system in leveraging unlabeled data, and its superiority remains consistent across various models and datasets.

We also present the time cost required to achieve different test accuracies in Fig. 5. FedMatch is excluded from the comparison plots on IMAGE-100 because it fails to achieve the target accuracy. When training small-scale models, our system fails to outperform all of the baselines on the SVHN dataset in terms of the time cost, as shown in Fig. 5(a). This happens when the cost of transmitting the features outweighs that of the entire model, as evidenced by the high overhead of the FedSwitch-SL. However, both FedSwitch-SL and our system benefit from scaling the size of the model. For instance, to achieve 80% accuracy on CIFAR-10, it takes 208.4 min and 217.9 min on average for our system and FedSwitch-SL to train an AlexNet, respectively, and 284.4-1308.0 min for other baselines on FL, which indicates speed-ups of 1.4-6.3 \times on the baselines. Moreover, for a higher target accuracy such as 85%, it takes 534.9 min for FedSwitch-SL, while other SemiFL baselines span from 652.3 to 2230.0 min. In contrast, our system only takes 406.1 min.

Additionally, our system speeds up training by 3.0-5.3 \times for reaching 60% test accuracy with VGG16 on the IMAGE-100 dataset compared to FedSwitch-SL and Semi-FL baselines, respectively. To investigate the secret of our training efficiency,

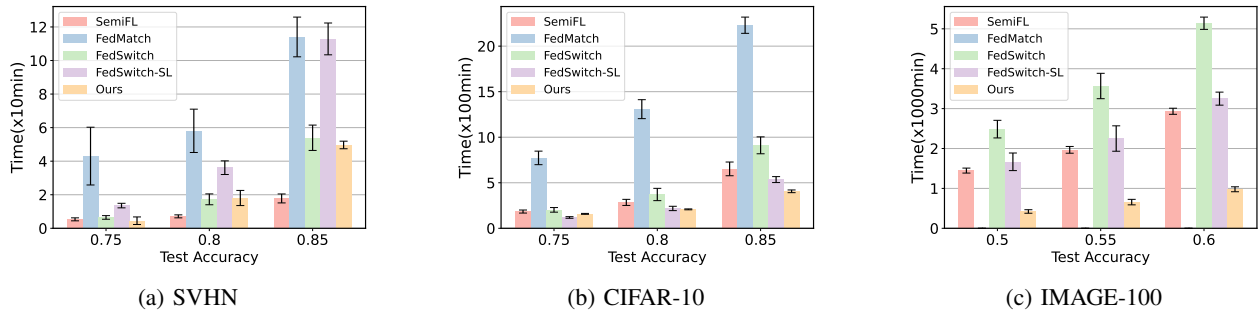


Fig. 5: Comparison of time cost on three datasets.

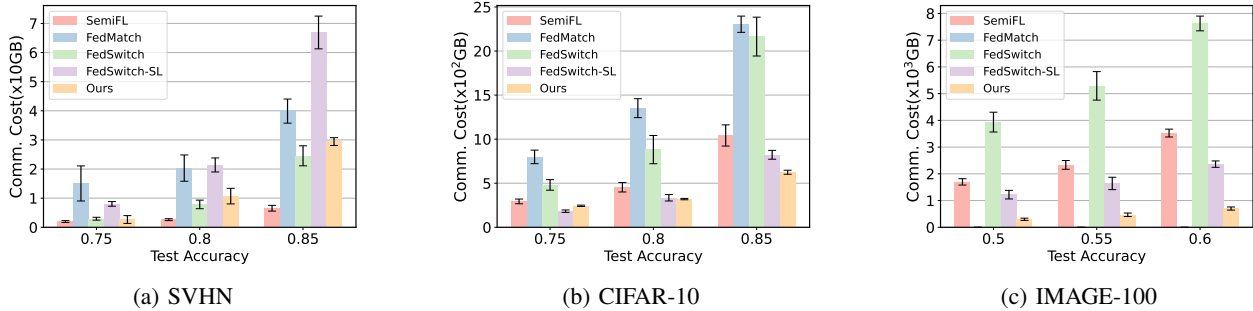


Fig. 6: Comparison of communication costs on three datasets.

TABLE III: Computation/Communication time ($\times 100$ min).

Baseline	Dataset		
	SVHN	CIFAR-10	IMAGE-100
SemiFL	3.3/0.2	5.8/11.9	16.2/29.3
FedMatch	4.7/0.3	10.3/13.7	21.7/24.0
FedSwitch	3.1/0.3	5.0/12.6	15.9/36.3
FedSwitch-SFL	1.2/2.6	3.2/9.1	13.7/18.2
Ours	2.2/3.1	3.0/9.5	14.2/19.0

TABLE IV: Test accuracy (%) on different datasets ($\alpha = 0.1$).

Baseline	Dataset		
	SVHN	CIFAR-10	IMAGE-100
SemiFL	80.5(0.66)	78.9(0.90)	50.8(1.69)
FedMatch	84.1(0.56)	79.7(0.96)	29.1(1.70)
FedSwitch	82.9(0.50)	79.4(0.61)	48.9(1.83)
FedSwitch-SL	83.0(0.65)	79.2(0.67)	49.3(1.58)
Ours	86.3(0.68)	83.4(0.66)	56.6(1.33)

we record the computing time on two alternate training phases and synchronization time (mainly includes communication) for all baselines in Table III. The results show that most of the time spent on training large-scale models is not on computation, but on communication, where the advantages of our system lie. We reduced much of the time for communication with the help of the SFL framework, but we do not stop there: the clustering regularization promotes the model convergence with little extra cost. This results in competitive time cost performance against Semi-FL works, in which performing complete training and model transmission has become a burden for clients.

2) *Effect of Communication Cost*: We demonstrate the communication efficiency of our proposed system through Fig. 6, which tracks the overall network traffic consumption until the target accuracy is reached. Our choice of split layers, as elaborated in Section V-D5, played a pivotal role in achieving this efficiency. Our system exhibits the least amount of network traffic consumption in most cases. For example, in Fig. 6(b), our system consumes only 319.9GB

to achieve 80% accuracy on CIFAR-10, while FedSwitch consumes 15.2GB higher and Semi-FL baselines consume from 454.1 to 1351.7GB. This translates to reductions of 4.5%-78.4% in communication costs. Similarly, Fig. 6(c) demonstrates that our system reduces communication cost by 70.3%-90.8% compared to all baselines, respectively, when reaching 60% test accuracy on IMAGE-100. The low communication cost of both FedSwitch-SL and our system implies the training efficiency of the SFL framework since the communication time is a significant contributor to the overall training time. However, in certain cases, such as training a customized CNN model, the transmission cost of features might outweigh the benefits of SFL. Fig. 6(a) shows that our system consumes approximately 10.7GB to achieve 85% accuracy is still 27.4% higher than FedSwitch.

3) *Adaptability to Data Distribution*: We compare our system with baselines dealing with data non-IIDness. This is implemented through sampling data from a Dirichlet distribution $Dir(\alpha)$ [42] for each client. The results are presented

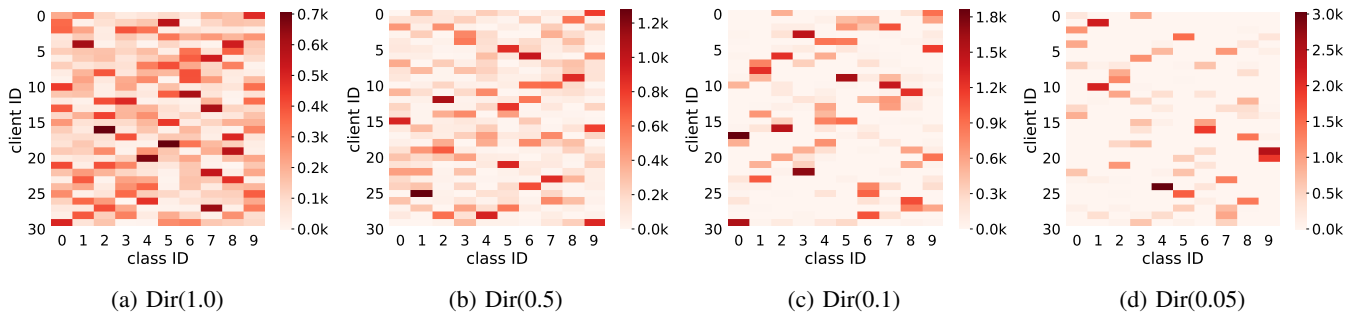


Fig. 7: Data distribution of each client with different non-IID levels.

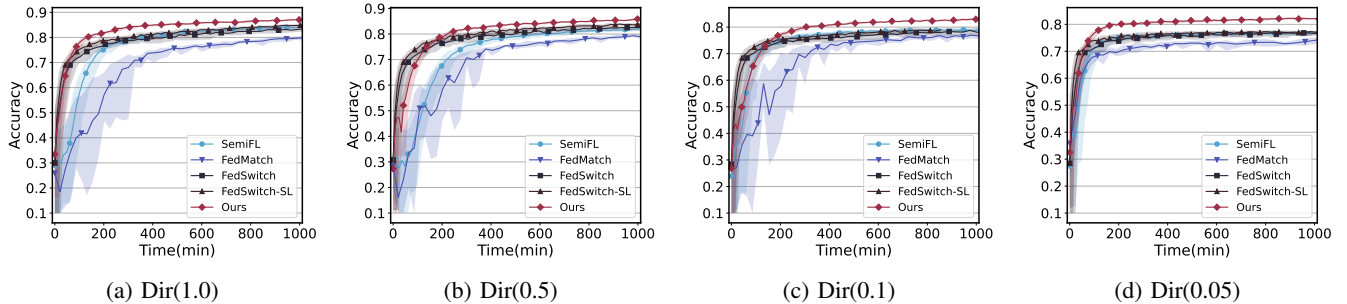


Fig. 8: Training process on different data distributions.

TABLE V: Test accuracy (%) of models on CIFAR-10 with different data distributions.

Baseline	Data distribution			
	Dir(1.0)	Dir(0.5)	Dir(0.1)	Dir(0.05)
SemiFL	84.9(0.92)	83.1(1.30)	78.9(0.90)	76.5(1.05)
FedMatch	85.9(1.03)	84.4(1.10)	79.7(0.96)	76.6(1.42)
FedSwitch	86.2(1.00)	83.8(1.14)	79.4(0.61)	77.3(0.99)
FedSwitch-SL	86.4(0.98)	84.1(0.65)	79.2(0.67)	77.2(1.07)
Ours	87.9(0.95)	86.2(1.29)	83.4(0.66)	82.4(0.89)

in Table IV, where different categories of data on each client follow a distribution of $Dir(0.1)$. From the results, our method achieves a consistent improvement over SemiFL and FedSwitch-SL on all three datasets. Concretely, our system outperforms SemiFL by 5.8%, 4.5%, and 5.8% on the three datasets, respectively. Besides, compared to FedSwitch-SL, we improve the test accuracy by 3.3%, 4.2%, and 7.3%, respectively. It demonstrates the effectiveness of our design in mitigating data non-IIDness, which is getting more significant on datasets with a wider variety of categories.

Moreover, we investigate the adaptability of our method on different data skewness on CIFAR-10. The data distributions among clients in our settings are shown in Fig. 7 and we present the training process on these distributions in Fig. 8. Notably, the performance of FedMatch fluctuates dramatically for around 400 minutes since it uses decomposed model parameters for supervised training and semi-supervised training, highlighting the detrimental effect of such disjoint

learning on model convergence. Table V provides a direct comparison of the final performance for different levels of non-IIDness. In some extreme cases, FedMatch performs similarly to Supervised-only, suggesting that even with multiple helpers for pseudo-labeling, the model parameters can still be misled by the highly skewed unlabeled dataset. A common phenomenon is that the more the data is skewed, the more the model performance deteriorates. In contrast, our system consistently achieves the highest accuracy across all levels of data skewness, showcasing its adaptability to diverse data distributions. Under extreme non-IID scenarios such as $Dir(0.05)$, the test accuracy of our system improves by 5.1%-5.9%, compared to all baselines. The experimental results align with our original intention well with the assistance of the clustering of teacher features. Notably, the results of SVHN and IMAGE-100 are in good agreement with those observed on CIFAR-10. Due to the limited space, we omit the experimental results here.

4) *Impact of the Scale of Labeled Dataset*: We conduct experiments on CIFAR-10, where we place 4,000 labeled data samples on the PS. However, in real-world scenarios, the amount of labeled data on the PS varies. To explore the impact of different scales of labeled datasets on our method, we conduct experiments by changing the amount of labeled data on the entire dataset. The results are presented in Fig. 9. We observe that the test accuracy gradually decreased from 87.9% to 63.0% when the amount of labeled data varied from 4,000 to 250 in FedSwitch-SL. To investigate the reason for the significant performance decline when the amount of labeled data decreased from 500 to 250, we record the mask rate (the

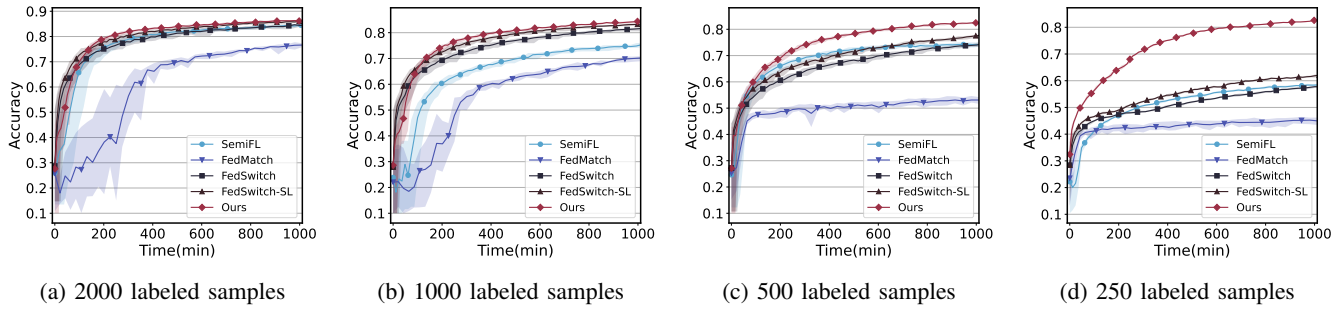


Fig. 9: Training process on different amounts of labeled data.

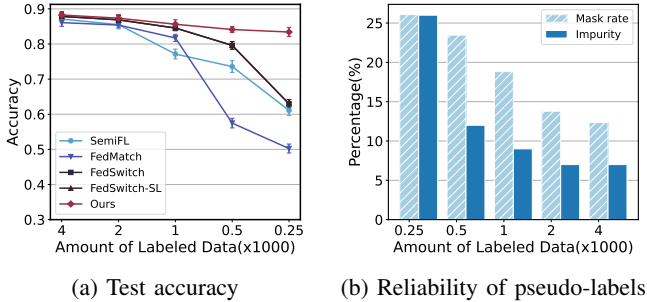


Fig. 10: Training performance varies with data scales.

number of examples that are masked out) and data impurity (the error rate of unlabeled data that falls above the threshold) of FedSwitch as an example in Fig. 10(b). We infer that this issue is attributed to the increase in both the mask rate and data impurity, causing the data to become unreliable.

By contrast, our system predominates the quality of predictions, as shown in Fig. 10(a), indicating the advantages of our proposed clustering regularization. Our method utilizes data samples with the largest class probability that fall beneath τ , which is considered invalid in consistency regularization. Moreover, supervised training on strong-augmented data provides a solid foundation for semi-supervised learning by enhancing model robustness, thus reducing impurities of unlabeled data. In addition, our results suggest that only a few labeled data (less than 2% of the overall dataset) is enough to satisfy some accuracy requirements, 80% for example.

5) *Impact of Split Layer*: Our choice of split layers for each model is primarily based on the cost of communication and computation on the client. Fig. 11 illustrates the impacts of split layer on communication cost, with $K_u = 50$ and batch size set to 64 on various datasets, except for IMAGE-100, which is set to 32 due to GPU memory constraints. The communication cost during each round is revealed as the sum of the size of features and the size of the bottom model. It is commonly known that the computation cost (floating-point operations) increases with the number of layers. However, this law does not hold for communication costs, as the size of the full model concentrates on the top full-connected layers, but the size of features is much larger in the first few layers than in the later ones. In fact, the minimum communication

cost may exist in the hidden layer, as shown in Fig. 11. For that, we prioritize the split layer with small-size features while ensuring it does not compromise the effectiveness of clustering regularization. Based on these considerations, the indices of the split layer we select are 2, 5, and 13 for CNN, AlexNet, and VGG16, respectively.

6) *Impact of Global Updating Frequency Adaptation*: We evaluate the impact of the global updating frequency adaptation algorithm on the performance of our approach. We present the comparison in Fig. 12 between our system with (w/) and without (w/o) the algorithm in terms of accuracy and training loss. The result shows that our adaptive adjustment of global updating frequency helps the model training reach an equilibrium closer to the global optima. This is consistent with our expectation in Section IV-A, with a noticeable increase in final accuracy. This effect is particularly evident when dealing with smaller amounts of unlabeled data. For instance, with 250 labeled data on the PS, the adaptation strategy improves accuracy by 8.7%, while the average global updating frequency is reduced to 32.5. Moreover, as seen in Fig. 12(b), adapting the global updating frequency brings a greater reduction in training loss, and the effect is especially obvious at several milestones that the global updating frequency decays. In contrast, with a constant global updating frequency ($=50$), the loss descent is hindered to a large extent because of the negative effect between our two training stages. Notably, the increase in the training loss during initial rounds is due to the increase in the amount of confident unlabeled data when the model performance is constantly improved with supervised training. In summary, our adaptation algorithm serves as a good complement to our proposed method.

VI. RELATED WORK

A. Federated Learning

Federated Learning (FL) has been proposed to perform privacy-preserving distributed model training [1], [43], [44]. In FL, data heterogeneity is a crucial factor for training performance, both in terms of accuracy and efficiency. Zhao *et al.* [9] demonstrate that the issue of accuracy reduction caused by non-IID data can be explained by weight divergence, and they address this issue by sharing a small subset of data between clients for local training, which raises concerns about data privacy. Li *et al.* [45] propose adding a proximal term to

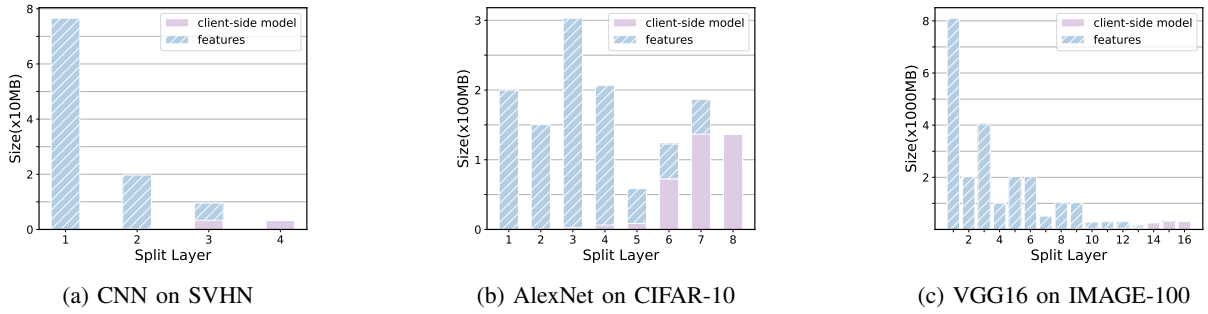


Fig. 11: Sizes of bottom model and features for different models regarding different split layers.

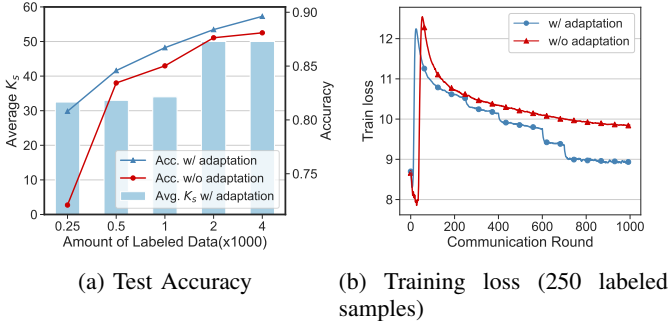


Fig. 12: Impact of global updating frequency adaptation.

the objective to improve convergence stability, but it introduces non-negligible computation burdens on clients. Recently, Li *et al.* [24] address the non-IID issue from a model representation perspective by correcting local updates with the representation of the global model. However, typical FL generally perform model training on labeled data, which is impractical in many real-world applications [46], [47].

B. Semi-Supervised Federated Learning

To utilize unlabeled data in FL, Semi-supervised Federated Learning (Semi-FL) has gained significant attention. It shares the objective of FL and extends to the semi-supervised learning setting. Some studies assume clients possess both labeled and unlabeled data [10]–[12] for their loss calculation. To relax the assumption of labeled data on clients, several approaches focus on more common scenarios where labeled data reside on the server. Diao *et al.* [16] present SemiFL, which applies Mixup technique [39] to augment the local dataset on clients and pioneer the alternate training phases widely adopted in later literature. Moreover, SemiFL achieves accuracy comparable with standalone training. Jeong *et al.* [17] introduce FedMatch, which enforces prediction consistency between clients to address non-IID challenges. To mitigate the high communication cost in sharing client models, Wang *et al.* [20] conduct knowledge distillation on the server, which requires a pre-trained model for the process. Concurrently, Zhao *et al.* [19] achieve state-of-the-art results by adaptively switching between teacher and student models for pseudo-labeling. Nonetheless, this method relies on an IIDness hyper-

parameter for system control, which might be inaccessible for new tasks or datasets.

C. Split Federated Learning

Split Federated Learning (SFL) [22] focuses on training large-scale models on resource-constrained end devices by incorporating the advantages of federated learning [1] and split learning. For instance, Thapa *et al.* [7] pioneer feasible SFL, which protects model privacy through model splitting and enables client-side model updates through exchanging of features/gradients. To reduce the traffic consumption, Han *et al.* [6] introduce an auxiliary network to update client-side models, without requiring gradients from the server. Then, Oh *et al.* [48] propose LocFedMix-SL, which uploads mixup-augmented features to the server for faster convergence and employs an auxiliary network to regularize the client-side models for better performance. To address system heterogeneity, Liao *et al.* [8] accelerates SFL on resource-constrained and heterogeneous clients by determining diverse batch sizes for different clients and adapting local updating frequency in each aggregation round. Recently, Han *et al.* [49] propose SplitGP to ensure both personalization and generalization capabilities by allocating different tasks for all clients. Despite these notable advancements, none of the existing SFL works have yet explored utilizing features to address the non-IID issue.

VII. CONCLUSION

In this paper, we have reviewed the distinct properties of SFL and proposed a novel Semi-SFL system to perform SFL with clustering regularization on unlabeled and non-IID client data. We have theoretically and experimentally investigated the impact of global updating frequency on model convergence. Then, we have developed a control algorithm for dynamically adjusting the global updating frequency, so as to mitigate the training inconsistency and enhance training performance. Extensive experiments have demonstrated that our system provides a 3.0 \times speed-up in training time and reduces the communication cost by about 70.3% while reaching the target accuracy, and achieves up to 5.1% improvement in accuracy under non-IID scenarios compared to the baselines.

REFERENCES

- [1] J. Konečný, H. B. McMahan, D. Ramage, and P. Richtárik, “Federated optimization: Distributed machine learning for on-device intelligence,” *arXiv preprint arXiv:1610.02527*, 2016.
- [2] B. Liang, J. Cai, and H. Yang, “A new cell group clustering algorithm based on validation & correction mechanism,” *Expert Systems with Applications*, vol. 193, p. 116410, 2022.
- [3] J. Wen, Z. Zhang, Y. Lan, Z. Cui, J. Cai, and W. Zhang, “A survey on federated learning: challenges and applications,” *International Journal of Machine Learning and Cybernetics*, vol. 14, no. 2, pp. 513–535, 2023.
- [4] L. Li, Y. Fan, M. Tse, and K.-Y. Lin, “A review of applications in federated learning,” *Computers & Industrial Engineering*, vol. 149, p. 106854, 2020.
- [5] D. Arpit, S. Jastrzębski, N. Ballas, D. Krueger, E. Bengio, M. S. Kanwal, T. Maharaj, A. Fischer, A. Courville, Y. Bengio *et al.*, “A closer look at memorization in deep networks,” in *International conference on machine learning*. PMLR, 2017, pp. 233–242.
- [6] D.-J. Han, H. I. Bhatti, J. Lee, and J. Moon, “Accelerating federated learning with split learning on locally generated losses,” in *ICML 2021 Workshop on Federated Learning for User Privacy and Data Confidentiality*. ICML Board, 2021.
- [7] C. Thapa, P. C. M. Arachchige, S. Camtepe, and L. Sun, “Splitfed: When federated learning meets split learning,” in *Proceedings of the AAAI Conference on Artificial Intelligence*, vol. 36, no. 8, 2022, pp. 8485–8493.
- [8] Y. Liao, Y. Xu, H. Xu, Z. Yao, L. Wang, and C. Qiao, “Accelerating federated learning with data and model parallelism in edge computing,” *IEEE/ACM Transactions on Networking*, 2023.
- [9] Y. Zhao, M. Li, L. Lai, N. Suda, D. Civin, and V. Chandra, “Federated learning with non-iid data,” *arXiv preprint arXiv:1806.00582*, 2018.
- [10] H. Lin, J. Lou, L. Xiong, and C. Shahabi, “Semifed: Semi-supervised federated learning with consistency and pseudo-labeling,” *arXiv preprint arXiv:2108.09412*, 2021.
- [11] W. Kim, K. Park, K. Sohn, R. Shu, and H.-S. Kim, “Federated semi-supervised learning with prototypical networks,” *arXiv preprint arXiv:2205.13921*, 2022.
- [12] L. Wang, Y. Xu, H. Xu, J. Liu, Z. Wang, and L. Huang, “Enhancing federated learning with in-cloud unlabeled data,” in *2022 IEEE 38th International Conference on Data Engineering (ICDE)*. IEEE, 2022, pp. 136–149.
- [13] T. Lin, L. Kong, S. U. Stich, and M. Jaggi, “Ensemble distillation for robust model fusion in federated learning,” *Advances in Neural Information Processing Systems*, vol. 33, pp. 2351–2363, 2020.
- [14] A. Albaseer, B. S. Ciftler, M. Abdallah, and A. Al-Fuqaha, “Exploiting unlabeled data in smart cities using federated edge learning,” in *2020 International Wireless Communications and Mobile Computing (IWCMC)*. IEEE, 2020, pp. 1666–1671.
- [15] Z. Zhang, Y. Yang, Z. Yao, Y. Yan, J. E. Gonzalez, K. Ramchandran, and M. W. Mahoney, “Improving semi-supervised federated learning by reducing the gradient diversity of models,” in *2021 IEEE International Conference on Big Data (Big Data)*. IEEE, 2021, pp. 1214–1225.
- [16] E. Diao, J. Ding, and V. Tarokh, “Semifl: Communication efficient semi-supervised federated learning with unlabeled clients,” *arXiv preprint arXiv:2106.01432*, 2021.
- [17] W. Jeong, J. Yoon, E. Yang, and S. J. Hwang, “Federated semi-supervised learning with inter-client consistency & disjoint learning,” in *9th International Conference on Learning Representations, ICLR 2021*. International Conference on Learning Representations, ICLR, 2021.
- [18] Z. Long, L. Che, Y. Wang, M. Ye, J. Luo, J. Wu, H. Xiao, and F. Ma, “Fedsiam: Towards adaptive federated semi-supervised learning,” *arXiv preprint arXiv:2012.03292*, 2020.
- [19] J. Zhao, S. Ghosh, A. Bharadwaj, and C.-Y. Ma, “When does the student surpass the teacher? federated semi-supervised learning with teacher-student ema,” *arXiv preprint arXiv:2301.10114*, 2023.
- [20] J. Wang, S. Zeng, Z. Long, Y. Wang, H. Xiao, and F. Ma, “Knowledge-enhanced semi-supervised federated learning for aggregating heterogeneous lightweight clients in iot,” in *Proceedings of the 2023 SIAM International Conference on Data Mining (SDM)*. SIAM, 2023, pp. 496–504.
- [21] X. Li, M. Jiang, X. Zhang, M. Kamp, and Q. Dou, “Fedbn: Federated learning on non-iid features via local batch normalization,” *arXiv preprint arXiv:2102.07623*, 2021.
- [22] O. Gupta and R. Raskar, “Distributed learning of deep neural network over multiple agents,” *Journal of Network and Computer Applications*, vol. 116, pp. 1–8, 2018.
- [23] K. Sohn, D. Berthelot, N. Carlini, Z. Zhang, H. Zhang, C. A. Raffel, E. D. Cubuk, A. Kurakin, and C.-L. Li, “Fixmatch: Simplifying semi-supervised learning with consistency and confidence,” *Advances in neural information processing systems*, vol. 33, pp. 596–608, 2020.
- [24] Q. Li, B. He, and D. Song, “Model-contrastive federated learning,” in *Proceedings of the IEEE/CVF Conference on Computer Vision and Pattern Recognition*, 2021, pp. 10713–10722.
- [25] D. Lee, S. Kim, I. Kim, Y. Cheon, M. Cho, and W.-S. Han, “Contrastive regularization for semi-supervised learning,” in *Proceedings of the IEEE/CVF Conference on Computer Vision and Pattern Recognition*, 2022, pp. 3911–3920.
- [26] P. Khosla, P. Teterwak, C. Wang, A. Sarna, Y. Tian, P. Isola, A. Maschinot, C. Liu, and D. Krishnan, “Supervised contrastive learning,” *Advances in Neural Information Processing Systems*, vol. 33, pp. 18661–18673, 2020.
- [27] K. Gupta, T. Ajanthan, A. v. d. Hengel, and S. Gould, “Understanding and improving the role of projection head in self-supervised learning,” *arXiv preprint arXiv:2212.11491*, 2022.
- [28] E. D. Cubuk, B. Zoph, J. Shlens, and Q. V. Le, “Randaugment: Practical automated data augmentation with a reduced search space,” in *Proceedings of the IEEE/CVF conference on computer vision and pattern recognition workshops*, 2020, pp. 702–703.
- [29] X. Li, K. Huang, W. Yang, S. Wang, and Z. Zhang, “On the convergence of fedavg on non-iid data,” *arXiv preprint arXiv:1907.02189*, 2019.
- [30] H. Yang, M. Fang, and J. Liu, “Achieving linear speedup with partial worker participation in non-iid federated learning,” *arXiv preprint arXiv:2101.11203*, 2021.
- [31] F. Haddadpour and M. Mahdavi, “On the convergence of local descent methods in federated learning,” *arXiv preprint arXiv:1910.14425*, 2019.
- [32] A. Ajallooeian and S. U. Stich, “On the convergence of sgd with biased gradients,” *arXiv preprint arXiv:2008.00051*, 2020.
- [33] E. Arazo, D. Ortego, P. Albert, N. E. O’Connor, and K. McGuinness, “Pseudo-labeling and confirmation bias in deep semi-supervised learning,” in *2020 International Joint Conference on Neural Networks (IJCNN)*. IEEE, 2020, pp. 1–8.
- [34] Y. Netzer, T. Wang, A. Coates, A. Bissacco, B. Wu, and A. Y. Ng, “Reading digits in natural images with unsupervised feature learning,” 2011.
- [35] A. Krizhevsky, G. Hinton *et al.*, “Learning multiple layers of features from tiny images,” 2009.
- [36] O. Russakovsky, J. Deng, H. Su, J. Krause, S. Satheesh, S. Ma, Z. Huang, A. Karpathy, A. Khosla, M. Bernstein *et al.*, “Imagenet large scale visual recognition challenge,” *International journal of computer vision*, vol. 115, pp. 211–252, 2015.
- [37] A. Krizhevsky, I. Sutskever, and G. E. Hinton, “Imagenet classification with deep convolutional neural networks,” *Communications of the ACM*, vol. 60, no. 6, pp. 84–90, 2017.
- [38] K. Simonyan and A. Zisserman, “Very deep convolutional networks for large-scale image recognition,” *arXiv preprint arXiv:1409.1556*, 2014.
- [39] D. Berthelot, N. Carlini, I. Goodfellow, N. Papernot, A. Oliver, and C. A. Raffel, “Mixmatch: A holistic approach to semi-supervised learning,” *Advances in neural information processing systems*, vol. 32, 2019.
- [40] Y. Xu, Y. Liao, H. Xu, Z. Ma, L. Wang, and J. Liu, “Adaptive control of local updating and model compression for efficient federated learning,” *IEEE Transactions on Mobile Computing*, 2022.
- [41] I. Loshchilov and F. Hutter, “Sgdr: Stochastic gradient descent with warm restarts,” *arXiv preprint arXiv:1608.03983*, 2016.
- [42] T.-M. H. Hsu, H. Qi, and M. Brown, “Measuring the effects of non-identical data distribution for federated visual classification,” *arXiv preprint arXiv:1909.06335*, 2019.
- [43] J. Liu, Y. Xu, H. Xu, Y. Liao, Z. Wang, and H. Huang, “Enhancing federated learning with intelligent model migration in heterogeneous edge computing,” in *2022 IEEE 38th International Conference on Data Engineering (ICDE)*. IEEE, 2022, pp. 1586–1597.
- [44] Z. Jiang, Y. Xu, H. Xu, Z. Wang, C. Qiao, and Y. Zhao, “Fedmp: Federated learning through adaptive model pruning in heterogeneous edge computing,” in *2022 IEEE 38th International Conference on Data Engineering (ICDE)*. IEEE, 2022, pp. 767–779.
- [45] T. Li, A. K. Sahu, M. Zaheer, M. Sanjabi, A. Talwalkar, and V. Smith, “Federated optimization in heterogeneous networks,” *Proceedings of Machine learning and systems*, vol. 2, pp. 429–450, 2020.

- [46] T.-Y. Lin, M. Maire, S. Belongie, J. Hays, P. Perona, D. Ramanan, P. Dollár, and C. L. Zitnick, "Microsoft coco: Common objects in context," in *Computer Vision—ECCV 2014: 13th European Conference, Zurich, Switzerland, September 6-12, 2014, Proceedings, Part V 13*. Springer, 2014, pp. 740–755.
- [47] A. Radford, J. Wu, R. Child, D. Luan, D. Amodei, I. Sutskever *et al.*, "Language models are unsupervised multitask learners," *OpenAI blog*, vol. 1, no. 8, p. 9, 2019.
- [48] S. Oh, J. Park, P. Vepakomma, S. Baek, R. Raskar, M. Bennis, and S.-L. Kim, "Locfedmix-sl: Localize, federate, and mix for improved scalability, convergence, and latency in split learning," in *Proceedings of the ACM Web Conference 2022*, 2022, pp. 3347–3357.
- [49] D.-J. Han, D.-Y. Kim, M. Choi, C. G. Brinton, and J. Moon, "Splitgp: Achieving both generalization and personalization in federated learning," in *IEEE INFOCOM 2023-IEEE Conference on Computer Communications*. IEEE, 2023, pp. 1–10.

A. Proof of Theorem 1

Theorem 1. The sequence of outputs $\{\mathbf{w}^{h,k}\}$ generated by supervised training and global aggregation satisfies:

$$\min_{h \in [H], k \in [K_s+1]} \mathbb{E} \|\nabla F(\mathbf{w}^{h,k})\|^2 \leq \frac{2(F(\mathbf{w}^0) - F(\mathbf{w}^*))}{\eta H K_s} + \Phi$$

where $\Phi \triangleq \left(\frac{L^2(K_u-1)(2K_u-1)\eta^2}{3K_s} + \frac{LK_u^2\eta^3}{K_s} + 1 \right) G_u^2 + (L\eta + \frac{2K_u}{K_s}) G_s^2$.

Proof: First, for model trained on the supervised stage, according to Lipschitz smoothness property in Assumption 1, we have:

$$\begin{aligned} & \mathbb{E}[F(\mathbf{w}^{h,k+1})] - \mathbb{E}[F(\mathbf{w}^{h,k})] \\ & \leq -\eta \mathbb{E} \langle \nabla F(\mathbf{w}^{h,k}), \tilde{\nabla} f_s(\mathbf{w}^{h,k}) \rangle + \frac{L\eta^2}{2} \mathbb{E} [\|\tilde{\nabla} f_s(\mathbf{w}^{h,k})\|^2] \end{aligned}$$

By using Lemma 5 and summing up K_s global iterations, we obtain:

$$\begin{aligned} & \mathbb{E}[F(\mathbf{w}^{h+\frac{1}{2}})] - \mathbb{E}[F(\mathbf{w}^h)] \\ & \leq \frac{1}{2} \eta \sum_{k=0}^{K_s-1} \mathbb{E} \|\nabla F(\mathbf{w}^{h,k})\|^2 + \frac{K_s(L\eta^2 G_s^2 + \eta G_u^2)}{2} \end{aligned}$$

For the model after aggregation, we have:

$$\begin{aligned} & \mathbb{E}[F(\mathbf{w}^{h+1})] - \mathbb{E}[F(\mathbf{w}^{h+\frac{1}{2}})] \\ & \leq -\mathbb{E} \langle \nabla F(\mathbf{w}^{h+\frac{1}{2}}), \Delta^h \rangle + \frac{L}{2} \mathbb{E} [\|\Delta^h\|^2] \\ & \stackrel{(a)}{=} -\eta \frac{K_u}{2} \mathbb{E} \|\nabla F(\mathbf{w}^{h+\frac{1}{2}})\|^2 + \frac{(K_u-1)(2K_u-1)L^2\eta^3 G_u^2}{6} \\ & \quad + \eta K_u G_s^2 + \frac{L}{2} \mathbb{E} [\|\Delta^h\|^2] \end{aligned}$$

where (a) follows Lemma 5.

By summing up all aggregation rounds, and from $F(\mathbf{w}^H) \leq \mathbb{E}[F(\mathbf{w}^*)]$, we can write:

$$\begin{aligned} & \frac{1}{H} \sum_{h=1}^H \mathbb{E} [K_u \|\nabla F(\mathbf{w}^{h+\frac{1}{2}})\|^2] + \sum_{k=0}^{K_s-1} \mathbb{E} \|\nabla F(\mathbf{w}^{h,k})\|^2 \\ & \leq \frac{2(F(\mathbf{w}^0) - F(\mathbf{w}^*))}{\eta H} \\ & \quad + \left(\frac{L^2(K_u-1)(2K_u-1)\eta^2}{3} + K_s + LK_u^2\eta \right) G_u^2 \\ & \quad + (LK_s\eta + 2K_u) G_s^2 \end{aligned}$$

Since $K_u > 0$, we have:

$$\begin{aligned} & \min_{h \in [H], k \in [K_s+1]} \mathbb{E} \|\nabla F(\mathbf{w}^{h,k})\|^2 \\ & \leq \frac{1}{HK_s} \sum_{k=1}^K \sum_{k=0}^{K_s} \mathbb{E} \|\nabla F(\mathbf{w}^{h,k})\|^2 \\ & \leq \frac{2(F(\mathbf{w}^0) - F(\mathbf{w}^*))}{\eta H K_s} + \Phi \end{aligned}$$

which completes the proof.

B. Key Lemmas

Lemma 1. For random variables X_1, \dots, X_r , we have:

$$\mathbb{E} [\|X_1 + \dots + X_r\|^2] \leq r \mathbb{E} [\|X_1\|^2 + \dots + \|X_r\|^2]$$

Lemma 2. For random vectors X, Y, Z , we have:

$$\mathbb{E} \langle X, Y + Z \rangle \geq \mathbb{E} \langle X, Y \rangle - \|\mathbb{E} \langle X, Z \rangle\|$$

Lemma 3. According to Assumption 2, we have:

$$\mathbb{E} \|\tilde{\nabla} f_{u,i}(\mathbf{w})\|^2 \leq G_u^2 \quad (1)$$

$$\|\nabla f_u(\mathbf{w})\|^2 \leq G_u^2 \quad (2)$$

$$\|\nabla f_s(\mathbf{w})\|^2 \leq G_s^2 \quad (3)$$

Proof: For Eq. (1):

$$\begin{aligned} & \mathbb{E} \|\nabla f_{u,i}(\mathbf{w})\|^2 \\ & \leq \frac{1}{|\mathcal{B}_{U,i}|} \sum_{x \in \mathcal{B}_{U,i}} \|\tilde{\nabla} f_{u,i}(\mathbf{w})\|^2 \\ & \stackrel{(b)}{\leq} G_u^2 \end{aligned}$$

where (a) is obtained by Lemma 1, (b) follows Assumption 2. Eq. (2) and Eq. (3) can be proved in a similar way.

Lemma 4. According to Assumptions 1 and 2, we have:

$$\begin{aligned} \mathbb{E} \langle \nabla f_u(\mathbf{w}^h), \Delta^h \rangle & \geq \frac{\eta K_u}{2} \mathbb{E} \|\nabla f_u(\mathbf{w}^h)\|^2 \\ & \quad - \frac{(K_u-1)(2K_u-1)L^2\eta^3 G_u^2}{6} \end{aligned}$$

where $\Delta^h \triangleq \frac{1}{N} \sum_{i=1}^N (\mathbf{w}_i^{h+1} - \mathbf{w}^h)$.

Proof:

$$\begin{aligned} & \mathbb{E} \langle \nabla f_u(\mathbf{w}^h), \Delta^h \rangle \\ & = \mathbb{E} \langle \nabla f_u(\mathbf{w}^h), \Delta^h - \eta K_u \nabla f_u(\mathbf{w}^h) + \eta K_u \nabla f_u(\mathbf{w}^h) \rangle \\ & \stackrel{(a)}{\geq} \eta K_u \mathbb{E} \|\nabla f_u(\mathbf{w}^h)\|^2 - \|\mathbb{E} \langle \nabla f_u(\mathbf{w}^h), \Delta^h - \eta K_u \nabla f_u(\mathbf{w}^h) \rangle\| \\ & \geq \eta K_u \mathbb{E} \|\nabla f_u(\mathbf{w}^h)\|^2 \\ & \quad - \|\mathbb{E} \langle \sqrt{\eta K_u} \nabla f_u(\mathbf{w}^h), \frac{\sqrt{\eta}}{\sqrt{K_u}} (\Delta^h - K_u \nabla f_u(\mathbf{w}^h)) \rangle\| \\ & \geq \eta K_u \mathbb{E} \|\nabla f_u(\mathbf{w}^h)\|^2 \\ & \quad - \frac{1}{2} (\eta K_u \mathbb{E} \|\nabla f_u(\mathbf{w}^h)\|^2 + \frac{\eta}{K_u} \mathbb{E} \|\frac{\Delta^h}{\eta} - K_u \nabla f_u(\mathbf{w}^h)\|^2) \end{aligned} \quad (4)$$

where (a) follows 2. Note that:

$$\Delta^h = \frac{1}{N} \sum_{i=1}^N \sum_{k=0}^{K_u-1} (\mathbf{w}_i^{h,k+1} - \mathbf{w}_i^{h,k}) = \frac{1}{N} \sum_{i=1}^N \sum_{k=0}^{K_u-1} \eta \tilde{\nabla} f_{u,i}(\mathbf{w}_i^{h,k})$$

We have:

$$\begin{aligned}
& \frac{\Delta^h}{\eta} - K_u \nabla f_u(\mathbf{w}^h) \\
&= \frac{1}{N} \sum_{i=1}^N \sum_{k=0}^{K_u-1} \tilde{\nabla} f_{u,i}(\mathbf{w}_i^{h,k}) - K_u \frac{1}{N} \sum_{i=1}^N \nabla f_{u,i}(\mathbf{w}^h) \\
&= \frac{1}{N} \sum_{i=1}^N \sum_{k=0}^{K_u-1} (\tilde{\nabla} f_{u,i}(\mathbf{w}_i^{h,k}) - \nabla f_{u,i}(\mathbf{w}^h)) \\
&= \frac{1}{N} \sum_{i=1}^N \sum_{k=0}^{K_u-1} (\nabla f_{u,i}(\mathbf{w}_i^{h,k}) - \nabla f_{u,i}(\mathbf{w}^h))
\end{aligned}$$

where the last equality follows Assumption 3. So we can bound $\mathbb{E} \|\frac{\Delta^h}{\eta} - K_u \nabla F(\mathbf{w}^h)\|^2$ as:

$$\begin{aligned}
& \mathbb{E} \|\frac{\Delta^h}{\eta} - K_u \nabla F(\mathbf{w}^h)\|^2 \\
&\leq \frac{L^2}{N} \sum_{i=1}^N \sum_{k=0}^{K-1} \mathbb{E} \|\mathbf{w}_i^{h,k} - \mathbf{w}_i^h\|^2 \\
&\stackrel{(a)}{=} \frac{L^2}{N} \sum_{i=1}^N \sum_{k=0}^{K-1} \mathbb{E} \|\sum_{m=0}^{k-2} \eta \tilde{\nabla} f_{u,i}(\mathbf{w}_i^{h,m})\|^2 \\
&\leq \frac{L^2 \eta^2}{N} \sum_{i=1}^N \sum_{k=0}^{K-1} ((k-1) \sum_{m=0}^{k-2} \mathbb{E} \|\tilde{\nabla} f_{u,i}(\mathbf{w}_i^{h,m})\|^2) \\
&\stackrel{(b)}{\leq} \frac{L^2}{N} \sum_{i=1}^N \sum_{k=1}^{K_u} ((k-1)^2 \eta^2 G_u^2) \\
&= \frac{K_u(K_u-1)(2K_u-1)L^2\eta^2 G_u^2}{6}
\end{aligned} \tag{5}$$

where (a) and (b) are obtained by Lemma 1 and follows Assumption 1, (c) follows Lemma 3.

Lemma 5. According to Assumptions 1 and 2, we have:

$$\mathbb{E} \langle \nabla F(\mathbf{w}^h), \tilde{\nabla} f_s(\mathbf{w}^h) \rangle \geq \frac{1}{2} \mathbb{E} \|\nabla F(\mathbf{w}^h)\|^2 - \frac{1}{2} G_u^2 \tag{6}$$

$$\begin{aligned}
\mathbb{E} \langle \nabla F(\mathbf{w}^{h+\frac{1}{2}}), \Delta^h \rangle &\geq \frac{\eta K_u}{2} \mathbb{E} \|\nabla F(\mathbf{w}^{h+\frac{1}{2}})\|^2 \\
&\quad - \frac{(K_u-1)(2K_u-1)L^2\eta^3 G_u^2}{6} - \eta K_u G_s^2
\end{aligned} \tag{7}$$

where $\Delta^h \triangleq \frac{1}{N} \sum_{i=1}^N (\mathbf{w}_i^{h+1} - \mathbf{w}_i^{h+\frac{1}{2}})$.

Proof: For Eq. (6), we have:

$$\begin{aligned}
& \mathbb{E} \langle \nabla F(\mathbf{w}^h), \tilde{\nabla} f_s(\mathbf{w}^h) \rangle \\
&\stackrel{(a)}{=} \mathbb{E} \langle \nabla F(\mathbf{w}^h), \nabla f_s(\mathbf{w}^h) \rangle \\
&= \mathbb{E} \langle \nabla F(\mathbf{w}^h), -\nabla f_u(\mathbf{w}^h) + \nabla F(\mathbf{w}^h) \rangle \\
&\stackrel{(b)}{\geq} \mathbb{E} \|\nabla F(\mathbf{w}^h)\|^2 - \|\mathbb{E} \langle \nabla F(\mathbf{w}^h), -\nabla f_u(\mathbf{w}^h) \rangle\|
\end{aligned}$$

where (a) follows Assumption 3, (b) comes from Lemma 2.

Note that $2\langle U, V \rangle \leq \|U\|^2 + \|V\|^2$, we obtain:

$$\begin{aligned}
& \|\mathbb{E} \langle \nabla F(\mathbf{w}^h), -\nabla f_u(\mathbf{w}^h) \rangle\| \\
&\leq \frac{1}{2} (\mathbb{E} \|\nabla F(\mathbf{w}^h)\|^2 + \mathbb{E} \|\nabla f_u(\mathbf{w}^h)\|^2) \\
&\leq \frac{1}{2} \mathbb{E} \|\nabla F(\mathbf{w}^h)\|^2 + \frac{1}{2} G_u^2
\end{aligned}$$

where the last inequality follows Lemma 1. According to the above inequalities, we have:

$$\mathbb{E} \langle \nabla F(\mathbf{w}^h), \tilde{\nabla} f_s(\mathbf{w}^h) \rangle \geq \frac{1}{2} \mathbb{E} \|\nabla F(\mathbf{w}^h)\|^2 - \frac{1}{2} G_u^2$$

which completes the proof of Eq. (6).

For Eq. (7), similar to Eq. (4), we have:

$$\begin{aligned}
& \mathbb{E} \langle \nabla F(\mathbf{w}^{h+\frac{1}{2}}), \Delta^h \rangle \\
&\geq \eta K_u \mathbb{E} \|\nabla F(\mathbf{w}^{h+\frac{1}{2}})\|^2 \\
&\quad - \frac{1}{2} (\eta K_u \mathbb{E} \|\nabla F(\mathbf{w}^{h+\frac{1}{2}})\|^2 + \frac{\eta}{K_u} \mathbb{E} \|\frac{\Delta^h}{\eta} - K_u \nabla F(\mathbf{w}^{h+\frac{1}{2}})\|^2)
\end{aligned}$$

By letting:

$$\begin{aligned}
X &= \frac{1}{N} \sum_{i=1}^N \sum_{k=0}^{K-1} (\tilde{\nabla} f_{u,i}(\mathbf{w}_i^{h,k}) - \nabla f_u(\mathbf{w}^{h+\frac{1}{2}})) \\
Y &= \frac{1}{N} \sum_{i=1}^N \sum_{k=0}^{K-1} (\nabla f_{u,i}(\mathbf{w}_i^{h+\frac{1}{2}}) - \nabla F(\mathbf{w}^{h+\frac{1}{2}}))
\end{aligned}$$

we have:

$$\frac{\Delta^h}{\eta} - K_u \nabla F(\mathbf{w}^{h+\frac{1}{2}}) = X + Y$$

So we bound $\mathbb{E} \|\frac{\Delta^h}{\eta} - K_u \nabla F(\mathbf{w}^{h+\frac{1}{2}})\|^2$ as:

$$\begin{aligned}
& \mathbb{E} \|\frac{\Delta^r}{\eta} - K_u \nabla F(\mathbf{w}^{h+\frac{1}{2}})\|^2 \\
&\leq 2\mathbb{E} \|X\|^2 + 2\mathbb{E} \|Y\|^2 \\
&\leq 2\mathbb{E} \|X\|^2 + 2K_u^2 G_s^2
\end{aligned}$$

where the above inequalities are obtained by Lemma 1 and Lemma 3. For $\mathbb{E} \|X\|^2$, it can be bounded as Eq. (5).

Putting the pieces together, we get:

$$\begin{aligned}
\mathbb{E} \langle \nabla F(\mathbf{w}^{h+\frac{1}{2}}), \Delta^h \rangle &\geq \frac{\eta K_u}{2} \mathbb{E} \|\nabla F(\mathbf{w}^{h+\frac{1}{2}})\|^2 \\
&\quad - \frac{(K_u-1)(2K_u-1)L^2\eta^3 G_u^2}{6} - \eta K_u G_s^2
\end{aligned}$$

which completes the proof.